Mineralogical Magazine, June 1999, Vol. 63(3), pp. 331–343

Concentric zoning patterns in crystallizing $(Cd,Ca)CO_3$ solid solutions from aqueous solutions

Á. Fernández-González and M. Prieto

Departamento de Geología, Universidad de Oviedo, 33005-Oviedo, Spain

A. Putnis

Institut für Mineralogie, Universität Münster, D-48149 Münster, Germany

S. López-Andrés

Departamento de Cristalografía y Mineralogía, Universidad Complutense, 28040-Madrid, Spain

ABSTRACT

Otavite-calcite solid solutions have been synthesized to investigate the factors which control the patterns of compositional zoning. The equilibrium partitioning of otavite between the aqueous and the solid phase can be described by means of a function $X_{CdCO_3}(X_{Cd,aq})_{eq}$, which relates the solid mole fraction and the aqueous activity fraction of Cd. According to this function, there is a strong preferential partitioning of Cd towards the solid. A set of experiments starting with parent solutions with different Cd^{2+}/Ca^{2+} ratios was carried out. In these experiments nucleation takes place at high supersaturations and the Cd^{2+} and Ca^{2+} ions tend to be laid down in a ratio which deviates from the equilibrium distribution. Experimental nucleation data can be fitted to a curve $X_{CdCO_3}(X_{Cd,aq})_{ef}$ of the same functionality as that for equilibrium.

After nucleation, supersaturation decreases as the crystals grow. During this process, substituting ions are not incorporated into the solid in the same stoichiometric proportion as in the aqueous solution. Therefore, crystal and fluid compositions tend to vary as growth proceeds and this evolution is registered as a compositional zoning. The curves $X_{CdCO_3}(X_{Cd,aq})_{eq}$ and $X_{CdCO_3}(X_{Cd,aq})_{ef}$ confine the reaction path corresponding to the growth process. Here, these curves are used to account for the observed zoning patterns.

Keywords: solid solution, otavite, calcite, crystal growth, zoning, oscillatory zoning.

Introduction

Considerable experimental work on the solid solution partitioning of divalent metal ions into calcite can be found in the geochemical literature. These works are of particular interest in the study of water-rock interactions that involve carbonate minerals and in environmental assessment of metal ion behaviour (Davis *et al*., 1987; Zachara *et al*., 1991; Stipp *et al*., 1992; Tesoreiro and Pankow, 1996). Chemically, a solid solution can occur when ions of one type substitute for ions of another type in a structure, forming a single crystalline phase. Otavite ($CdCO_3$) and calcite ($CaCO_3$), in particular, form a complete solid-solution series (Chang and Brice, 1971), where Cd^{2+} ions substitute for Ca^{2+}. This is not surprising if one considers the similarity of ionic radii for Ca^{2+} (1 Å) and Cd^{2+} (0.95 Å). Both end-members are rhombohedral $R\bar{3}c$ carbonates, with a lattice parameter a_0 (using the hexagonal axial system) which varies with composition in a linear way, from 4.93 Å to 4.99 Å (Borodin *et al*., 1979). The parameter c_0 varies in a similar way, although there is a small deviation from a linear relationship. Therefore, one would expect the formation of a nearly ideal solid solution. Calculations of the excess Gibbs energy by Königsberger *et al*. (1991) lead to the conclusion that the otavite-calcite solid solution series has ideal mixing properties.

Although intermediate phases of $(Cd,Ca)CO_3$ are not observed in nature, this system is of interest from the point of view of the sorption (and subsequent solid solution formation) of trace metals at the surface of carbonate minerals (Davis *et al*., 1987; Stipp *et al*., 1992). Cadmium is not naturally abundant at the Earth's surface, but in certain regions anthropogenic activities have increased concentrations in water and soils to dangerous levels (Nriagu, 1980). Laboratory and field studies indicate that sorption onto the surface of calcareous materials, represent a potentially significant Cd-removing process in aquatic, marine and groundwater environments. Currently, the geochemical models proposed for sorption of Cd^{2+} rely primarily on surface adsorption processes (accumulation of matter at the interface without the development of a three dimensional molecular arrangement). However, the growth of a layer of solid solution on the surface of the calcite substrate has recently been considered as the fundamental mechanism of Cd-sorption on the surface of calcite crystals (Tesoreiro and Pankow, 1996; Chiarello *et al*., 1997). Following these authors, if calcite is present, precipitation of Cd^{2+} as a carbonate solid solution will always occur, even when Cd^{2+} is present at trace levels, due to the strong tendency of this ion to partition into calcite.

In spite of the numerous studies on the $(Cd,Ca)CO_3$-H_2O system, the fundamental controls on ion partitioning during crystal growth remain poorly understood. While a thermodynamic approach is very useful, the importance of studying the crystallization behaviour in a kinetic or mechanistic framework is becoming more and more apparent (Paquette and Reeder, 1995). The experiments conducted here illustrate the crystallization behaviour of this solid solution. Crystallization experiments were carried out by counter-diffusion of reactants through a column of porous silica hydrogel. In these experiments the crystallization process has been studied by considering nucleation and growth separately. Nucleation takes place at high supersaturations (Prieto *et al*., 1994), and the Cd^{2+} and Ca^{2+} ions tend to be laid down in a ratio which deviates from the equilibrium distribution coefficient. After nucleation, supersaturation decreases as the crystals grow. During this process, substituting ions are not incorporated in the solid in the same stoichiometric proportion as in the aqueous solution. Therefore, crystal and aqueous solution compositions tend to vary as growth proceeds and this evolution is recorded in the crystal as a concentric compositional pattern. Moreover, as a consequence of the supersaturation decrease, the distribution coefficient evolves during the growth process from the nucleation value towards a value characteristic of equilibrium.

Numerous examples of concentric compositional zoning have been documented in a variety of carbonates, especially in natural calcites and dolomites (Reeder, 1986). Concentric zoning is produced when the interface (the limit between two growth bands) across which the change in composition occurs, coincides with an existing or prior growth surface. Therefore, these zoning patterns can provide a detailed record of the growth process. Concentric zoning delineates former growth surfaces and provides a record of the crystal morphology and of the temporal changes in the physicochemical conditions in existence during crystallization. In the present paper we report observations of concentric zoning in $(Cd,Ca)CO_3$ crystals grown from different parent solutions. From these patterns, the growth history of the crystals can be observed retrospectively, and those factors which are influenced by the evolution in the bulk fluid composition can be separated from those which promote the development of oscillatory zoning. We show that oscillatory zoning in these experiments is not associated with an oscillating bulk fluid composition but with local fluctuations inherent in the growth process under certain conditions.

Experimental

The technique used to grow the zoned calcite-otavite crystals is shown in Fig. 1, where parent aqueous solutions of two reagents are separated by a column of silica hydrogel (length 28 cm) in a U-shaped tube. The method has been extensively used as a way of growing crystals of sparingly soluble salts from aqueous solutions (Henisch, 1988). The gel was prepared by acidification with HCl (1 N) of a sodium silicate (Na_2SiO_3) solution (Merck, sp. gr.: 1.059 gcm^{-3}; pH 11.2) to the desired pH (5.5). Then the acidified solution was poured into the U-tube, where it polymerizes to a solid gel. The gel so-obtained is a porous medium which contains 95.6 wt% water within interconnecting pores, and NaCl as a soluble by-product. Within the gel structure the solution is stagnant because it is trapped within micron-sized pores (Henish, 1988). Solution convection is

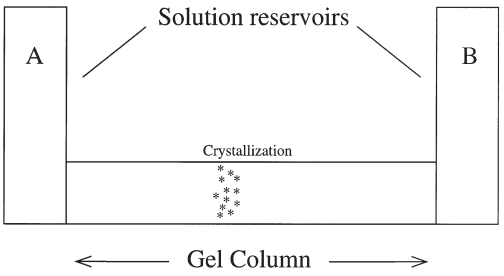

FIG. 1. Schematic representation of the experimental U-tube arrangement.

therefore completely depressed and mass transfer can take place only via molecular diffusion. To obtain (Cd,Ca)CO_3 crystals, the source reservoirs A and B were filled with 8 cm^3 of $CdCl_2$-$CaCl_2$ and Na_2CO_3 parent solutions, respectively. The initial concentrations of the solutions used are shown in Table 1. The experiments were carried out at 25 $\pm$ 0.1°C.

Before the experiment starts, the gel column is an homogeneous medium with zero reagent concentration. However, as a result of the diffusion of the reagents, the column becomes non-homogeneous and develops concentration and pH gradients. Finally, the counter-diffusing reacting ions meet and precipitate in a narrow region of the diffusion column, where a certain supersaturation threshold is first overstepped. The nucleation behaviour was studied by monitoring the precipitate location, the nucleation density and the experimental waiting period (the time taken for the first crystallites to become visible under magnification $\times$ 500). The experiments were stopped one month after nucleation. The crystals were extracted from the gel and confirmed to be members of the otavite-calcite series by X-ray powder diffraction (Philips PW1729-1710). To observe the compositional zoning within the crystals, they were cut, polished, carbon-coated, and studied by backscattered electron (BSE) imaging in a JEOL scanning microscope. Variations in composition lead to variations in image brightness (Lloyd, 1987), which allow inhomogeneities and compositional zoning to be visible. Detailed quantitative analyses and compositional profile lines of the crystal sections were obtained by electron microprobe (CAMEBAX SX50).

To characterize the crystallization behaviour completely, one must know the compositional evolution of both growing crystals and interstitial aqueous solution. Unfortunately, the evolution of the fluid composition in the crystallization region can only be followed until the nucleation event. After nucleation the compositional evolution of the crystals, and not that of the crystallizing fluid is recorded. For this reason, nucleation and growth are considered separately here, the latter requiring an interpretative model which put

TABLE 1. Nucleation data for the system (Cd,Ca)CO_3-H_2O. Columns 4 and 5 show the equilibrium and nucleation total activity products of the aqueous solution, according to Eqn (1), respectively. Columns 6 and 7 show the aqueous activity fraction (Eqn (4)) and the solid phase mole fraction corresponding to the nucleation time, respectively

Parent solutions						
$CdCl_2$(M)	$CaCl_2$(M)	Na_2CO_3(N)	$-\log \Sigma\Pi_{eq}$	$-\log\Sigma\Pi_{eff}$	$X_{Cd,aq}$	X_{CdCO_3}
0.00	0.5	0.5	8.48	5.37	0.000	0.00
0.01	0.5	0.5	10.05	5.66	0.010	0.20
0.03	0.5	0.5	10.11	5.40	0.015	0.54
0.05	0.5	0.5	10.28	5.50	0.022	0.63
0.10	0.5	0.5	10.46	5.44	0.025	0.79
0.20	0.5	0.5	10.75	5.46	0.051	0.81
0.30	0.5	0.5	10.98	5.45	0.082	0.82
0.40	0.5	0.5	11.11	5.44	0.103	0.86
0.50	0.5	0.5	11.21	5.44	0.133	0.89
0.50	0.3	0.5	11.46	5.64	0.235	0.94
0.50	0.2	0.5	11.78	5.92	0.481	0.96
0.50	0.1	0.5	11.95	6.06	0.712	0.98
0.10	0.0	0.5	12.10	6.21	1.000	1.00

limitations on the hypothetical reaction path, as we will discuss below.

In order to study the nucleation behaviour, special attention was paid to the composition of the initial nuclei. For each experimental run, the core of ten different individuals was analysed. The values of the solid mole fraction for the Cd-end-member displayed in Table 1 are mean values of these ten compositions. Dispersions from the mean values were always within a compositional rank lower than 0.1. The composition of the interstitial aqueous solution at nucleation was determined by following a 'protocol' fully described in previous papers (Prieto *et al*., 1994; 1997). This involves carrying out separate mass-transfer experiments (in which no reaction occurs) for each reactant over specified periods of time. Here, the concentration evolution in the nucleation region was determined by terminating diffusion experiments at 100 h intervals, removing the gel from the column and slicing the nucleation region, previously known from the crystallization experiments. This slice was then chemically analysed. Finally, to determine the actual concentration of the interstitial solutions, the measured concentrations were referred to as the effective volume of aqueous solution per gel volume unit (0.956 ± 0.002 cm^3 of solution per 1 cm^3 of gel). The Cd-content was analysed by atomic absorption spectrophotometry (UNICAM SP90), and the total amount of C was measured by means of a C-N-S elemental analyser (Carlo-Erba Na 1500). A set of mass-transfer experiments was carried out for each of the initial conditions displayed in Table 1. The pH evolution was determined in separate experiments by adding pH liquid indicator (Merck) to the sodium silicate solution during the gel preparation. As a result of the diffusion of the reagents, the pH evolves along the column, and it can be monitored by observing the development of changes in colour.

Analytical values of concentration as a function of time measured from mass-transfer experiments were fitted to second order polynomials by the least squares method and, from these polynomials, the concentrations of the chemical constituents at the nucleation time (previously known from crystallization experiments) were interpolated. Correlation coefficients were >0.99 in all cases. Finally, a Debye-Hückel aqueous speciation model was used to compute the activities of the main aqueous species from the analytical data. Here, the following aqueous species were considered: Cd^{2+}, $CdOH^+$, $Cd(OH)_3^-$, Cd_2OH^{3+}, $CdHCO_3^+$, $Cd(CO_3)_2^{2-}$, Ca^{2+}, $CaOH^+$, $CaHCO_3^+$, Na^+, HCO_3^-, $NaCO_3^-$, H^+, CO_3^{2-}, Cl^-, OH^-, $H_2CO_3^o$, $NaHCO_3^o$, $NaOH^o$, $CaCO_3^o$, $NaCl^o$, $Cd(OH)_2^o$, and $CdCO_3^o$.

Equilibrium and nucleation behaviour: reaction path limits for growth

The aqueous solubility of a solid solution may be described by the partial solubility products of the end-members. With this aim, Lippmann (1980) developed the concept of 'total activity product' $\Sigma\Pi$. In the case of the $(Cd,Ca)CO_3$ solid solution, $\Sigma\Pi$ is given by:

$$\Sigma\Pi = \left([Cd^{2+}] + [Ca^{2+}]\right)[CO_3^{2-}] \qquad (1)$$

where $[Cd^{2+}]$, $[Ca^{2+}$, and $[CO_3^{2-}]$ are the activities of the ions in the aqueous solution. At thermodynamic equilibrium the 'total solubility product' $\Sigma\Pi_{eq}$ of a solid solution, expressed as a function of the solid composition yields to the Lippmann's 'solidus' relation:

$$\Sigma\Pi_{eq} = K_{CdCO_3} X_{CdCO_3} \gamma_{CdCO_3} + K_{CaCO_3}, X_{CaCO_3} \gamma_{CaCO_3} \qquad (2)$$

where K_{CdCO_3}, X_{CdCO_3}, and γ_{CdCO_3} are, respectively, the solubility product, the solid mole fraction, and the solid phase activity coefficient of the component $CdCO_3$. Analogous symbols label these parameters for the component $CaCO_3$.

Lippmann also defined the 'solutus' equation which expresses $\Sigma\Pi_{eq}$ as a function of the aqueous solution composition:

$$\Sigma\Pi_{eq} = \frac{1}{\frac{X_{Cd,aq}}{X CdCO_3 \gamma_{CdCO_3}} + \frac{X_{Ca,aq}}{X CaCO_3 \gamma_{CaCO_3}}} \qquad (3)$$

where $X_{Cd,aq}$ is the aqueous activity fraction of Cd^{2+} in the aqueous solution, given by:

$$X_{Cd,aq} = \frac{[Cd^{2+}]}{[Cd^{2+}] + [Ca^{2+}]} \qquad (4)$$

An analogous expression defines $X_{Ca,aq}$.

In the case of the calcite-otavite solid solution, the Lippmann relationships can be computed by using end-members pK's of 8.48 for calcite (Plummer and Busenberg, 1982) and 12.1 for otavite (Stipp *et al*., 1993) and assuming an ideal solid solution (Königsberger *et al*., 1991). Lippmann's 'solidus' and 'solutus' relations can be plotted and used to predict the solubility of any solid solution in a similar way as binary-solid/

binary-melt phase diagrams (Glynn *et al*., 1990). Moreover, from Eqns 2 and 3, making γ_{CdCO_3} and γ_{CaCO_3} equal to 1 (ideal solid solution) and taking $X_{Ca,aq} = 1 - X_{Cd,aq}$ and $X_{CaCO_3} = 1 - X_{CdCO_3}$, the following expression can be deduced (Prieto *et al*., 1997):

$$X_{CdCO_3} = \frac{K_{CaCO_3} X_{Cd,aq}}{(K_{CaCO_3} - K_{CdCO_3}) X_{Cd,aq} + K_{CdCO_3}} \quad (5)$$

This last expression can be used to construct a $X_{Cd,aq}$–X_{CdCO_3} plot, which describes the coexisting compositions of solid and aqueous solution under equilibrium conditions (Fig. 2*a*). In this case, as the solid solution is considered ideal, the curve in Fig. 2*a* is symmetric in relation to the straight line joining the points (0,1) and (1,0). According to the Lippmann equations, the extremely low solubility of otavite compared to that of calcite involves a strong preferential partitioning of $CdCO_3$ in the solid phase. Aqueous solutions in equilibrium with Ca-rich solids are essentially free of Cd^{2+}. As Fig. 2*a* shows, only a very narrow range of aqueous compositions can coexist in equilibrium with intermediate solid solutions. The solids tend to be either Ca-rich (X_{CdCO_3}<0.1) or Cd-rich (X_{CdCO_3}>0.9) over a very small range of fluid compositions (0.000027 < $X_{Cd,aq}$ < 0.002154). This fact imposes a bimodal trend in crystallizing (Cd,Ca)CO_3 solid solutions (Prieto *et al*., 1997).

The $X_{Cd,aq}$–X_{CdCO_3} plot in Fig. 2*a* illustrates the distribution of the substituting ions between the aqueous and the solid phase, at thermodynamic equilibrium. This distribution is usually expressed in terms of the distribution coefficient:

$$D_{Cd} = \frac{X_{CdCO_3}}{X_{CaCO_3}} / \frac{[Cd^{2+}]}{[Ca^{2+}]} \quad (6)$$

In the case of an ideal solid solution, the equilibrium distribution coefficient is given by the ratio of the solubility products of the end-members. In this case, D_{Cd} takes a value of 4168.41, which again demonstrates a strong preferential partitioning for Cd towards the solid phase.

However, all experimental data show that precipitation begins under disequilibrium conditions, when a certain supersaturation level has been reached. This fact is specially evident when crystallization occurs in a porous medium. Porous media are very effective at suppressing nucleation (Putnis *et al*., 1995) and, as a consequence, precipitation always begins at a high supersaturation. To illustrate this fact, the total activity products, corresponding to equilibrium and to the composition of the aqueous phase at nucleation,

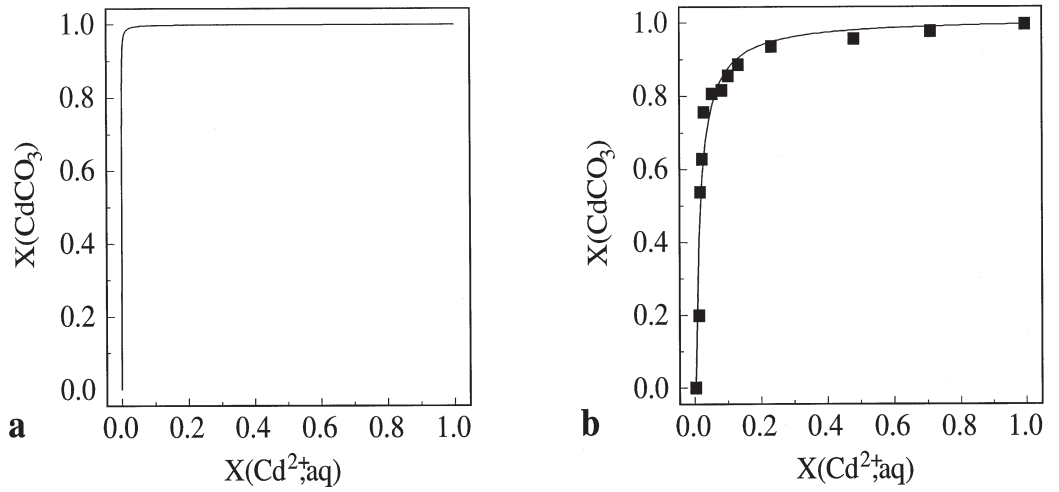

FIG. 2. (*a*) Equilibrium $X_{Cd,aq}$–X_{CdCO_3} plot according to Eqn (5). (*b*) Experimental $X_{Cd,aq}$–X_{CdCO_3} pairs at the nucleation time (data points from cols. 6 and 7 in Table 1). A curve fitting the experimental points has been computed according to Eqn (7).

are displayed in Table 1 (columns 4 and 5, respectively). The values are several orders of magnitude higher than the corresponding equilibrium values. Obviously, the composition of the crystals nucleating at such a supersaturation depends on kinetic factors, and the 'effective' distribution coefficients differ from the equilibrium values. This is clear if one observes the data points plotted on a $X_{Cd,aq}$–X_{CdCO_3} diagram (Fig. 2*b*). The corresponding experimental values are compiled in Table 1 (columns 6 and 7). It is worth noting that as in the equilibrium curve in Fig. 2*a*, the experimental data points in Fig. 2*b* show a symmetric configuration in relation to the straight line joining the points (0,1) and (1,0). This is due to the ideal character of the calcite-otavite solid solution.

Although the effective composition of the nucleating crystals deviates from the equilibrium values, data points in Fig. 2*b* can be fitted to a curve of the same functionality as Eqn 4. (Prieto *et al*.; 1997), i.e. to a function of the type:

$$X_{CdCO_3} = \frac{P_1 X_{Cd,aq}}{(P_1 - P_2)X_{Cd,aq} + P_2} \qquad (7)$$

where P_1 and P_2 are used as variable fitting parameters. In this case the best fit was obtained for $-\log P_1 = 9.65$ and $-\log P_2 = 11.47$.

By comparing the curve $X_{CdCO_3}(X_{Cd,aq})$ for equilibrium to that for nonequilibrium at nucleation, an obvious conclusion follows: the curvature of the non-equilibrium fitting function is smaller than that corresponding to the equilibrium plot. This means that preferential partitioning is in some way 'softened' at high supersaturation. Although a strong preferential partitioning remains, the solid solution is slightly less sensitive to changes in the fluid composition than is the equilibrium curve. The nuclei tend to be either Ca-rich ($X_{CdCO_3}<0.1$) or Cd-rich ($X_{CdCO_3}>0.9$) over a very small range of fluid compositions ($0.0015<X_{Cd,aq}<0.12$), but this range is significantly wider than the equilibrium one ($0.000027<X_{Cd,aq}<0.002154$). Moreover, if one considers the analogy between Eqns. 5 and 7, the 'effective distribution coefficient' $D_{Cd,eff}$ can be computed from the quotient between the fitting parameters P_1 and P_2. $D_{Cd,eff}$ takes a value of 66.094, which is notably smaller than the equilibrium value. This value is also smaller than the values obtained by Tesoreiro and Pankow (1996) in non-equilibrium conditions. These authors determine experimentally the dependence of the distribution coefficients on the growth rate, and obtained values ranging between 3041 (at low growth rates) and 201 (at high growth rates). The lower preferential partitioning in the present experiments is easily explained if the high deviations from equilibrium attained in a gel medium are considered. At high supersaturation values, there is less chance for thermodynamically-based selectivity effects to be exerted, and so the measured $D_{Cd,eff}$ values will decrease towards 1 as supersaturation becomes large.

In addition to this visualization of the nonequilibrium effect, the importance of the curves in Fig. 2*b* lies in which they confine the possible reaction paths for the growth process. Supersaturation at nucleation is the maximum supersaturation that will be attained during the crystallization process. After nucleation, supersaturation decreases as the crystals grow. Therefore, on the $X_{Cd,aq}$–X_{CdCO_3} plot, the reaction path corresponding to the growth process must lie between the equilibrium curve and the curve fitting the nucleation points (Fig. 3). Therefore, both curves confine the attainable distribution coefficients during crystallization.

Crystal growth and compositional zoning

As soon as stable nuclei have been formed from the supersaturated solution, they begin to grow into crystals of visible size. During this process

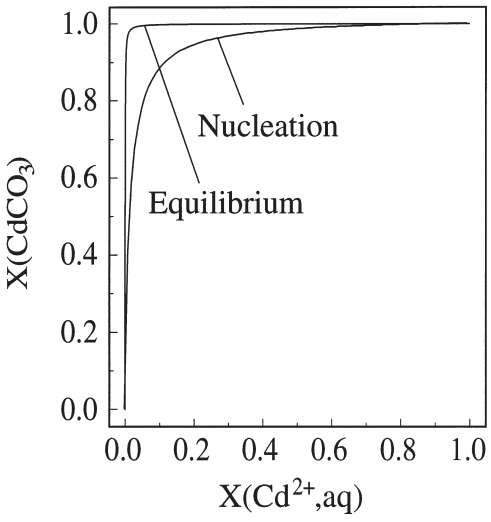

FIG. 3. Reaction path limits for growth.

substituting ions are not incorporated into the solid in the same stoichiometric proportion as in the aqueous solution. Therefore, crystal and aqueous solution compositions tend to vary as growth proceeds. The individual crystals grow in such a way that the layers growing on the surface block the inner zones from contact with the solution. This results in a compositional heterogeneity from core to rim in the bulk crystal. At the same time, the compositions of the growing crystals have a striking effect on their morphology. The compositional evolution is followed by a morphological evolution which can be monitored from the 'internal morphologies' of the crystalline individuals. The final morphology of the crystals depends on their compositional evolution which, in turn, is a result of the initial concentrations of the parent solutions. In the following paragraphs, we describe the growth behaviour of Cd-rich crystals and thereafter the effect produced by the progressive increase of Ca^{2+} in the fluid.

Figure 4*a* shows the morphology of a (Cd,Ca)CO_3 crystal obtained starting with 0.5 M $CdCl_2$ and 0.1 M $CaCl_2$ parent solutions (as shown in Table 1, the Na_2CO_3 parent solutions were 0.5 M in all cases). The shape is clearly dominated by the cleavage rhombohedron $\{10\bar{1}4\}$, but the polyhedral morphology is disturbed by preferential growth along certain directions, which breaks the singular character of the crystalline faces. As shown in Fig. 4*a*, the crystals are better faceted near the edges that meet at the two corners of the rhombohedron which are connected by the axis $\bar{3}$. There is also a trend to form overgrowth layers near these corners. For each face, only the two edges that converge at the axis $\bar{3}$ are clearly defined. The centre of the faces appears rough and depressed, and the development of the $\{10\bar{1}4\}$ facets is restricted to these edges. When observed from the $\bar{3}$ axis, the equatorial region of the crystals has a curved appearance, with inlets and outlets alternating every 60°. In the limiting case, the crystals develop morphologies with starlike contours. Some crystals are slightly elongated along the axis $\bar{3}$, with well-developed rhombohedral faces at both extremes and a curved equatorial region. These morphologies are very common in crystals with calcite-type structure grown at high supersaturations (Franke *et al*., 1979; Prieto *et al*., 1981; Heijnen, 1985; Fernández-Díaz *et al*., 1996).

From a compositional point of view, the surfaces of these crystals are rich in Ca, with a Cd-mol fraction <0.1 in all cases. As a whole, however, the compositions of the crystals are Cd-rich. Figure 4*b* shows the backscattered electron image of the central section of a typical crystal. The central 'white' region is Cd-rich with values of X_{CdCO_3} near unity (0.98 in the central nucleus). The compositional profile line shows a gradual decrease in X_{CdCO_3} from core to rim inside this white region, but in the transition zone the Cd-content decreases dramatically (0.1 mole-fraction/μm), to reach values <0.1 in the grey region.

The external morphology of the crystals changes when the Ca concentration in the parent solution is increased. Figure 4*c* shows the shape of a typical crystal grown from a 0.5 M $CdCl_2$ + 0.2 M $CaCl_2$ parent solution. This morphology is similar to that previously described, but the curved region is wider and shows a depressed equatorial zone. Moreover, most of the crystals show terraced surface structures which are formed by $\{10\bar{1}4\}$ facets. The backscattered electron image of the section of a typical crystal again shows two well-differentiated regions (Fig. 4*d*). The central 'white' region is Cd-rich, with X_{CdCO_3} near unity (an average value of 0.96 in the central nucleus). The grey, Ca-rich, region is, however, wider in this case.

The width of the Ca-rich region increases and the whole Cd-content decreases when the relative concentration of calcium in the parent solution is increased. Again, the compositional gradient in the zone of transition between Cd-rich and Ca-rich regions is extremely high (0.09 mole-fraction/μm), whereas it is more gradual inside these regions.

Starting with a equimolar parent solution (0.5 M $CdCl_2$ + 0.5 M $CaCl_2$), the crystals show some new features. Figure 4*e* shows the external morphology of a typical crystal. The crystals are peanut-shaped, with subparallel rhombohedral facets. The curved region is quite depressed and shows a wavy cleft with peaks and troughs alternating every 60°, thus reproducing the symmetry $\bar{3}$. In spite of this external appearance, the backscattered electron image shows that we are dealing with a single crystal (Fig. 4*f*). The central white region has a clearly rhombohedral outline. However, during the growth process the crystal becomes Ca-rich, and its morphology begins to be disturbed. The composition isolines, with the same grey intensity, allow us to follow this morphological evolution. As can be observed from the compositional profile line, the crystal shows again a central region, Cd-rich, with a

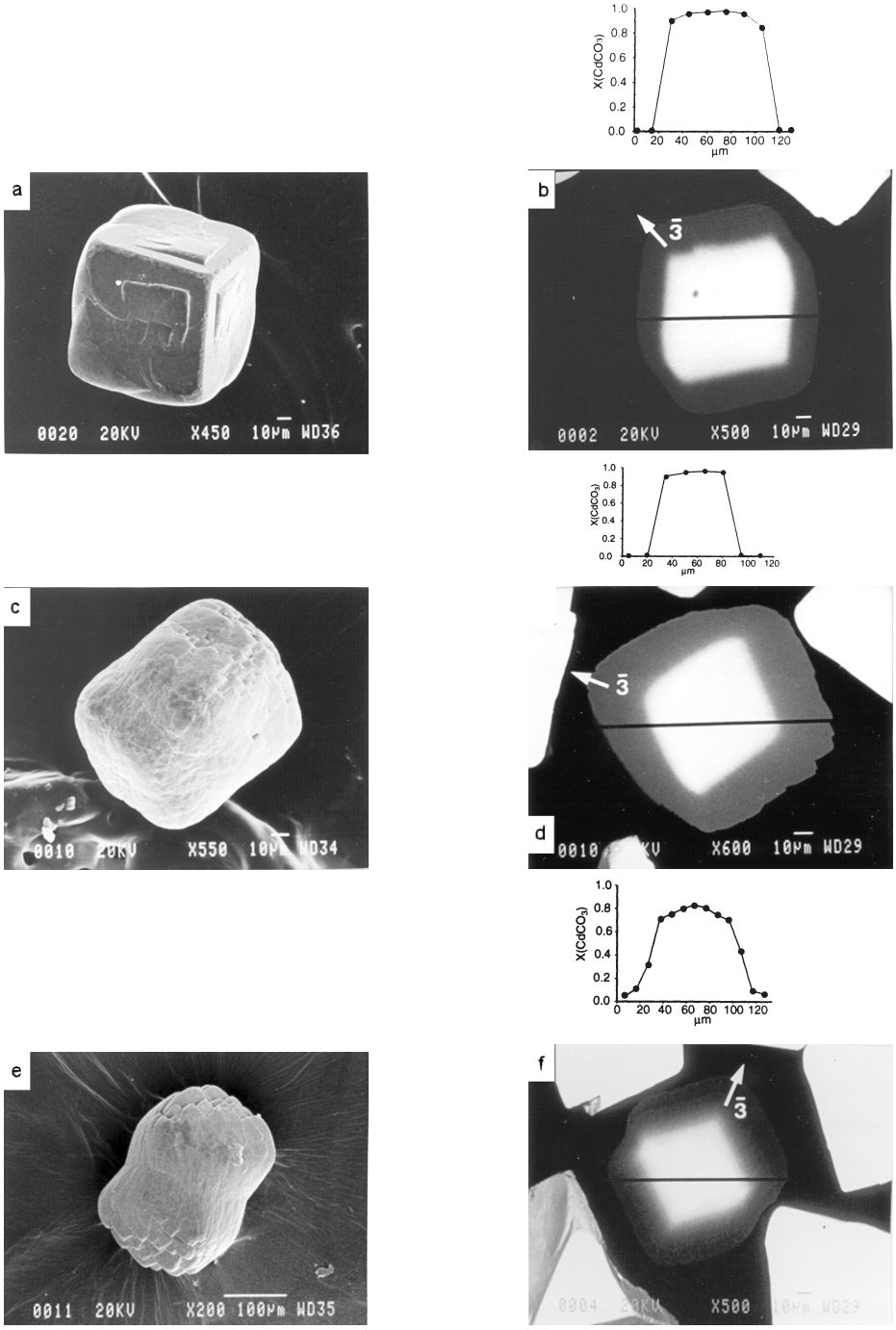

FIG. 4. (*a*), (*c*) and (*e*) Morphologies of $(Cd,Ca)CO_3$ crystals obtained from parent solutions 0.5 M $CdCl_2$ + 0.1 M $CaCl_2$, 0.5 M $CdCl_2$ + 0.2 M $CaCl_2$, and 0.5 M $CdCl_2$ + 0.5 M $CaCl_2$, respectively. (*b*), (*d*) and (*f*) Backscattered electron images and compositional profile lines of central sections of the crystals shown in (*a*), (*c*) and (*e*), respectively.

sharp transition towards the outer Ca-rich region. However, superimposed on this general gradient of composition, smaller compositional oscillations become visible. The overall gradient is similar in all the crystalline individuals of the experiment, but there is no correlation in the number of sub-zones for different crystals.

Crystals obtained from a non-equimolar parent solution with a concentration of Ca higher than that of Cd (0.2 M $CdCl_2$ + 0.5 M $CaCl_2$) show a central nucleus still Cd-rich, but the average X_{CdCO_3} value (0.81) is smaller than that of the preceding cases, and the compositional gradient in the region of transition is smaller. The Ca-rich region is wider and shows clear oscillatory zoning.

This trend develops further when the relative concentration of Ca in the parent solution is further increased. Figure 5*b* shows the central section of a crystal grown from a 0.05 M $CdCl_2$ + 0.5 M $CaCl_2$ parent solution. The growth still begins with a Cd-rich stage, but the $CdCO_3$ mole-fraction always take values <0.65. The $CdCO_3$ mole-fraction decreases from core to rim, but the gradient in the region of maximum slope is smaller than in the previous cases (0.03 mole-fraction/μm). Again, the Cd-rich region seems to be homogeneous, but in the Ca-rich region there are many compositional oscillations. The oscillatory, concentric zoning has a repeat distance ranging from 1 to 10 μm, and the amplitude of the oscillations is up to 0.25 in Cd mole-fraction. Moreover, whereas the whole compositional gradient is similar in all the crystals of the experiment, there is no correlation between specific zoning patterns for different crystals. This fact is common to all the experiments in which oscillatory zoning has been observed, and, as we will discuss below, is the key to interpreting this phenomenon.

Figure 5*c* shows the morphology of a typical crystal grown from a 0.03 $CdCl_2$ + 0.5 M $CaCl_2$ parent solution. As can be observed, this further decrease in the relative amount of Cd in the parent solution further disturbs the external morphology of the crystals. The individuals exhibit split-growth and a deep wavy cleft with peaks and troughs reproduces the $\bar{3}$ symmetry. The back-scattered electron image of a central section is shown in Fig. 5*d*. Although at the nucleation time the Cd^{2+} aqueous activity fraction was ~0.01, the nuclei are relatively Cd-rich (X_{CdCO_3} ~0.54), as a consequence of the strong preferential partitioning of Cd towards the solid phase. The Cd concentration decreases from core to rim, with a gradient of 0.015 mole-fraction/μm in the region of maximum slope. Although the amplitude of the compositional oscillations is smaller than in previous cases, the oscillatory zoning in the Ca-rich region can still be observed by increasing the image contrast.

When the relative concentration of Cd^{2+} in the parent solution is still smaller (0.01 M $CdCl_2$ + 0.5 M $CaCl_2$), the split crystal growth is more striking and begins at earlier stages of the growth process (Fig. 5*e*). Again one can observe two well-differentiated regions in the backscattered electron image (Fig. 5*f*). The white region is richer in Cd, although in this case X_{CdCO_3} is always <0.2. The Ca-rich region exhibits a clear oscillatory zoning that can be followed through the different sections of the crystal aggregate.

Summing up, the increase of the relative concentration of Ca in the parent solution disturbs the external morphology of the crystals. At the same time one can observe a progressive increase of the crystal size with the bulk Ca content. So, whereas Ca-poor crystals reach sizes of ~100 μm (see Fig. 4*a*), Ca-rich crystals reach, on average, sizes >5 times larger in the same growth period (Fig. 5*e*). This fact relates to the nucleation density which decreases as the Ca concentration is increased.

Discussion

As discussed previously using the $X_{Cd,aq}$–X_{CdCO_3} plot (Fig. 3), the reaction path corresponding to the growth process must lie between the equilibrium curve and the curve fitting the nucleation points. Within these limits, the evolutionary trajectory of the system will depend on the starting point, i.e. on the fluid composition at the nucleation time.

For instance, starting with 0.5 M $CdCl_2$ and 0.1 M $CaCl_2$ parent solutions the value of $X_{Cd,aq}$ at the nucleation time was 0.712. However, the strong preferential partitioning of Cd toward the solid phase leads to formation of nuclei with X_{CdCO_3} = 0.98, i.e. virtually free of Ca. As a result, near the crystals, the aqueous phase is strongly depleted in Cd^{2+} as growth proceeds. However, as the reaction path of the system must remain confined within the limits defined by the $X_{Cd,aq}$–X_{CdCO_3} curves, this evolution of the fluid composition does not give rise to significant changes in the solid composition. As shown in Fig. 6*a*, the crystal will continue to grow more Cd-rich until the region of maximum

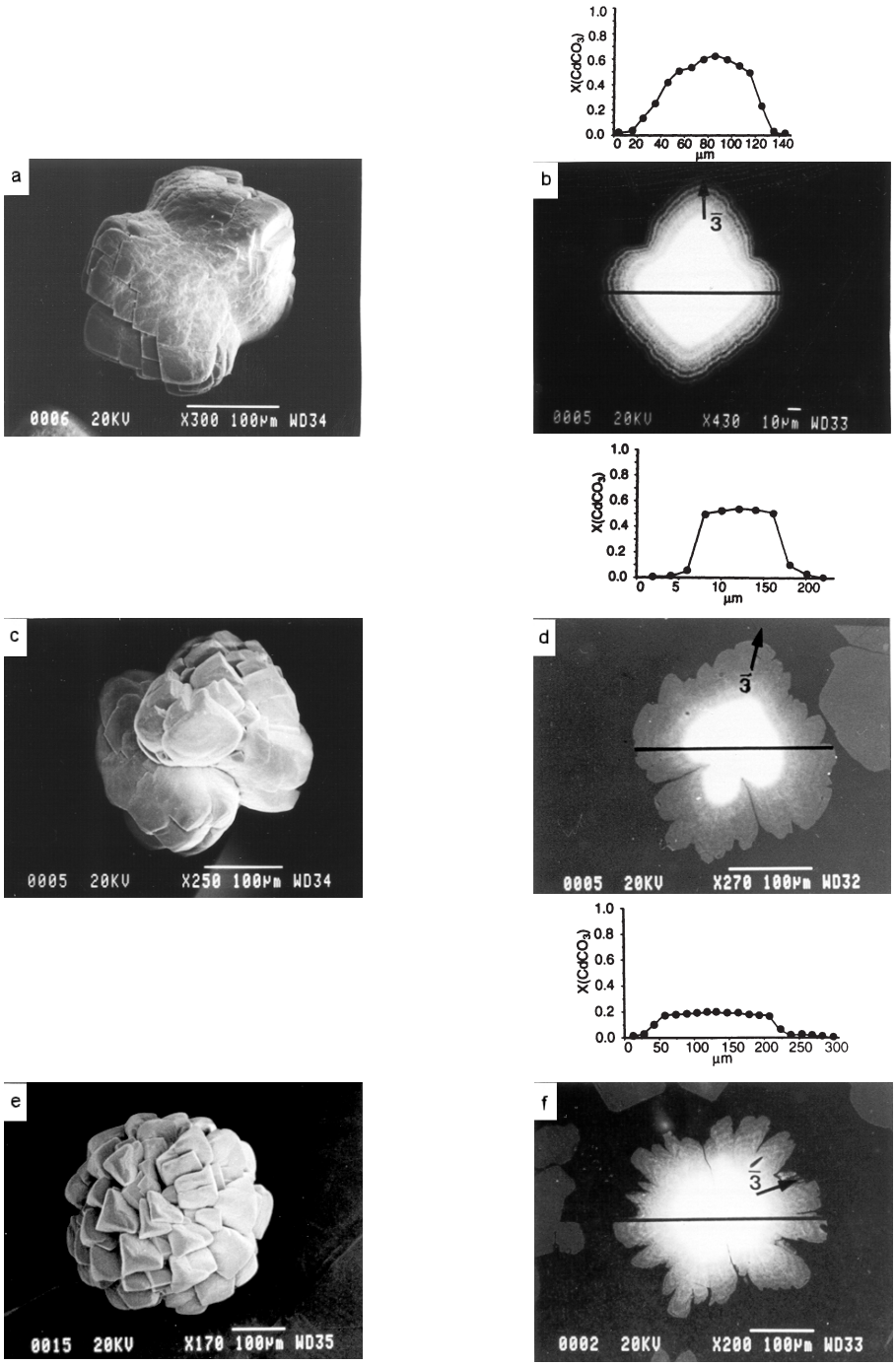

FIG. 5. (*a*), (*c*) and (*e*) Morphologies of $(Cd,Ca)CO_3$ crystals obtained from parent solutions 0.05 M $CdCl_2$ + 0.5 M $CaCl_2$, 0.03 M $CdCl_2$ + 0.5 M $CaCl_2$, and 0.01 M $CdCl_2$ + 0.5 M $CaCl_2$, respectively. (*b*), (*d*) and (*f*) Backscattered electron images and compositional profile lines of central sections of the crystals shown in (*a*), (*c*) and (*e*), respectively.

curvature of the curves is overpassed. Beyond this critical region the curves become almost vertical, and small variations in the fluid composition involve dramatic changes in the solid composition. The solid proceeds to grow more Ca-rich, and a concentric zoning of high gradient is produced (Fig. 4*b*).

Figure 6*b* shows a similar trajectory when the experiments start from parent solutions 0.5 M $CdCl_2$ + 0.2 M $CaCl_2$ (Table 1). At the nucleation time the fluid is less rich in Cd^{2+} than in the previous case ($X_{Cd,aq}$ = 0.481), but preferential partitioning leads again to Cd-rich nuclei (X_{CdCO_3} = 0.96). However, the reaction path followed by the system until it reaches the region of maximum curvature is shorter, and the external Ca-rich zone is wider (see Fig. 4*d*).

When the relative concentration of Ca in the parent solution is further increased (0.5 M $CdCl_2$ + 0.5 M $CaCl_2$) the fluid composition at the nucleation time is poor in Cd^{2+} ($X_{Cd,aq}$ = 0.133). The nuclei are still Cd-rich (X_{CdCO_3} = 0.89), but in this case the starting point is closer to the vertical side of the curve (Fig. 6*c*). As a consequence, the solid becomes Ca-rich from the early stages of the growth process. The fluid depletes in Cd^{2+} in a more gradual way, and the compositional gradients in the solid are less sharp (Fig. 4*f*).

For the experiments shown in Fig. 5, the reaction path is confined between the vertical segments of the curves. The crystals always show a higher Cd-content in the early stages, increasing progressively in Ca during the growth process. All crystals in Fig. 5 show oscillatory zoning. As we discussed above, these concentric subzones represent minor compositional fluctuations superimposed on the whole gradient. It is worth noting that oscillatory zoning only becomes apparent in the Ca-rich zone. The reason is obvious if one observes the $X_{Cd,aq}$–X_{CdCO_3} curves: when the composition of the aqueous solution at nucleation is rich in Ca^{2+} ($X_{Cd,aq}$<0.1; Table 1), the starting point is on the vertical branch of the curves. In this region the 'sensitivity' of the solid chemistry for small changes in the fluid composition is extreme. Therefore, any cause that provokes small fluctuations in the fluid composition will be 'recorded' in an amplified way in the solid.

A second feature of this oscillatory behaviour is the absence of correlation between specific zoning patterns for two nearby crystals of the same precipitate. This means that these minor compositional variations do not correspond to global changes in the bulk solution, but to periodic instabilities inherent in the growth process (Putnis *et al*., 1992; Prieto *et al*., 1993; Jamtveit *et al.*, 1995; Shore and Fowler, 1996). In the present experiments, this phenomenon could be explained as being due to non-linearities caused by coupling of growth parameters such that chemical variations arise spontaneously (Putnis *et al*., 1992; Ortoleva *et al*., 1987). Oscillatory-zoned crystals represent the material record of a 'chemical oscillator' (Gray and Scott, 1990).

Different models have been proposed in the literature to interpret oscillatory zoning in minerals (Allègre *et al*., 1981; Ortoleva *et al*., 1987; Reeder *et al*., 1990; Wang and Merino, 1992). Following these authors, the development of oscillatory patterns requires the coupling of at least two time-dependent variables through some sort of feedback mechanism. However, proposing a specific feedback mechanism (and a dynamic model based on it) for the present experiments is beyond the scope of this work. Here, we only wish to point out that oscillatory zoning only

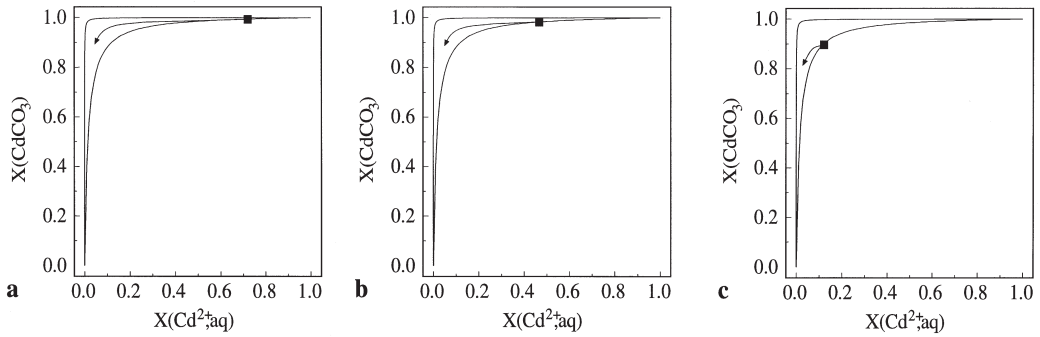

FIG. 6. Hypothetical reaction paths in the (Cd,Ca)CO_3-H_2O system for three different parent solutions: (*a*) 0.5 M $CdCl_2$ + 0.1 M $CaCl_2$, (*b*) 0.5 M $CdCl_2$ + 0.2 M $CaCl_2$, and (*c*) 0.5 M $CdCl_2$ + 0.5 M $CaCl_2$.

becomes apparent in the Ca-rich region, where small variations in the fluid composition imply dramatic changes in the solid composition, and the amplitude of the compositional waves is accordingly high. A later paper will deal with the analysis of these zoning patterns in terms of Lyapounov exponents (Halden, 1996).

Acknowledgements

This work was supported by DGES (Dirección General de Enseñanza Superior, Spain; Grant PB96-0550) and by the German/Spanish Joint Research Programme (HA1997-0126).

References

Allègre, C.J., Provost, A. and Jaupart C. (1981) Oscillatory zoning: A pathological case of crystal growth. *Nature*, **294**, 223–8.

Borodin, V.L., Lyntin, V.I., Ilyukhin, V.V. and Belov, N.V. (1979) Isomorphous calcite-otavite series. *Soviet Phys. Dokl.*, **24**, 226–7.

Chang, L.L.Y. and Brice, W.R. (1971) Subsolidus phase relations in the system calcium carbonate-cadmium carbonate. *Amer. Mineral.*, **56**, 338–41.

Chiarello, R.P., Sturchio, N.C., Grace, J.D., Geissbuhler, P., Sorensen, L.B., Cheng, L. and Xu, S. (1997) Otavite-calcite solid-solution formation at the calcite-water interface studied in situ by synchrotron X-ray scattering. *Geochim. Cosmochim. Acta*, **61**, 1467–74.

Davis, J.A., Fuller, C.C. and Cook, A.D. (1987) A model for trace metal sorption processes at the calcite surface: Adsorption of Cd^{2+} and subsequent solid solution formation. *Geochim. Cosmochim. Acta*, **51**, 1477–90.

Fernández-Díaz, L. Putnis, A., Prieto, M. and Putnis, C. (1996) The role of magnesium in the crystallization of calcite and aragonite in a porous medium. *J. Sed. Res*., **66**, 482–91.

Franke, W., Ittyachen, M.A. and Mohanan Pillai, K. (1979) Scanning electron microscopic studies on different habits of gel grown manganese carbonate crystals. *Pramãna*, **13**, 293–97.

Glynn, P.D., Reardon, E.J., Plummer, L.N. and Busenberg, E. (1990) Reaction paths and equilibrium end-points in solid-solution aqueous-solution systems. *Geochim. Cosmochim. Acta*, **54**, 267–82.

Gray, P. and Scott, S.K. (1990) *Chemical Oscillations and Instabilities: Non-linear Chemical Kinetics*. Oxford University Press, UK.

Halden, N.M. (1996) Determination of Lyapounov exponents to characterize the oscillatory distribution of trace elements in minerals. *Canad. Mineral.*, **34**, 1127–35.

Heijnen, W.M.M. (1985) The morphology of gel grown calcite. *Neues Jahrb. Mineral. Mh.*, 357–71.

Henisch, H.K. (1988) *Crystals in Gels and Liesegang Rings*. Cambridge University Press, UK.

Jamtveit B., Ragnarsdottir, K.V. and Wood, J. (1995) On the origin of zoned grossular-andradite garnets in hydrothermal systems. *Eur. J. Mineral.*, **7**, 1399–410.

Königsberger, E., Hausner, R. and Gamsjäger, H. (1991) Solid-solute phase equilibria in aqueous solution. V: The system $CdCO_3$-$CaCO_3$-H_2O. *Geochim. Cosmochim. Acta*, **55**, 3505–14.

Lippmann, F. (1980) Phase diagrams depicting aqueous solubility of binary carbonate systems. *Neues Jahrb. Mineral. Abh.*, **139**, 1–25.

Lloyd G.E. (1987) Atomic number and crystallographic contrast images with the SEM: A review of backscattered electron techniques. *Mineral. Mag.*, **51**, 3–19.

Nriagu, J.O. (1980) *Cadmium in the Environment, Part I. Ecological Cycling.* Wiley-Interscience, New York.

Ortoleva, P., Merino, E., Moore C. and Chadam, J. (1987) Geochemical self-organization I: Reaction-transport feedbacks and modeling approach. *Amer. J. Sci.*, **287**, 979–1007.

Paquette, J. and Reeder, R.J. (1995) Relationships between surface structure, growth mechanism, and trace element incorporation in calcite. *Geochim. Cosmochim. Acta*, **59**, 735–49.

Plummer, L.N. and Busenberg, E. (1982) The solubilities of calcite, aragonite and vaterite in CO_2–H_2O solutions between 0 and 90°C, and an evaluation of the aqueous model for the system $CaCO_3$-CO_2-H_2O. *Geochim. Cosmochim. Acta*, **46**, 1011–40.

Prieto, M., García-Ruiz, J.M. and Amorós, J.L. (1981) Growth of calcite crystals with non-singular faces. *J. Cryst. Growth*, **52**, 864–7.

Prieto, M., Putnis, A. and Fernández-Díaz, L. (1993) Crystallization of solid solutions from aqueous solutions in a porous medium: zoning in $(Ba,Sr)SO_4$. *Geol. Mag.*, **130**, 289–99.

Prieto, M., Putnis, A. Fernández-Díaz, L. and López-Andrés, S. (1994) Metastability in diffusing-reacting systems. *J. Cryst. Growth*, **142**, 225–35.

Prieto, M., Fernández-González, A. Putnis, A. and Fernández-Díaz, S. (1997) Nucleation, growth and zoning phenomena in crystallizing $(Ba,Sr)CO_3$, $Ba(SO_4,CrO_4)$, $(Ba,Sr)SO_4$, and $(Cd,Ca)CO_3$ solid solutions from aqueous solutions. *Geochim. Cosmochim. Acta*, **61**, 3383–97.

Putnis, A. Fernández-Díaz, L. and Prieto, M. (1992) Experimentally produced oscillatory zoning in the $(Ba,Sr)SO_4$ solid solution. *Nature*, **358**, 743–5.

Putnis, A., Prieto, M. and Fernández-Díaz, L. (1995) Fluid supersaturation and crystallization in porous media. *Geol. Mag.*, **132**, 1–13.

Reeder, R.J. (1986) Zoning types and their origins in sedimentary carbonate minerals. In *Geochemistry of the Earth's Surface* (R. Rodríguez and Y. Tardy, eds). pp. 740–52. Consejo Sup. Invest. Científicas, Centre Nat. Recher. Scientifique.

Reeder, R.J., Fagioly, R.O. and Meyers, W. (1990) Oscillatory zoning of Mn in solution grown calcite crystals. *Earth Sci. Rev.*, **29**, 39–46.

Shore, M. and Fowler, A.D. (1996) Oscillatory zoning in minerals, a common phenomenon. *Canad. Mineral.*, **34**, 1111–26.

Stipp, S.L., Hochella, M.F., Parks, G.A. and Leckie, J.O. (1992) Cd^{2+} uptake by calcite, solid state diffusion, and the formation of solid solution: Interface processes observed with near-surface sensitive techniques (XPS, LEED, and AES). *Geochim. Cosmochim. Acta*, **56**, 1941–54.

Stipp, S.L., Parks, G.A., Norddstrom, D.K. and Leckie, J.O. (1993) Solubility-product constant and thermodynamic properties for synthetic otavite, $CdCO_{3(s)}$, and aqueous association constants for the Cd(II)-CO_2-H_2O system. *Geochim. Cosmochim. Acta*, **57**, 2699–713.

Tesoreiro, A.J. and Pankow, J.F. (1996) Solid solution partitioning of Sr^{2+}, Ba^{2+}, and Cd^{2+} to calcite. *Geochim. Cosmochim. Acta*, **60**, 1053–63.

Wang, Y. and Merino, E. (1992) Dynamic model of oscillatory zoning of trace elements in calcite: Double layer, inhibition, and self-organization. *Geochim. Cosmochim. Acta*, **56**, 587–96.

Zachara, J.M., Cowan, C.E. and Resch, C.T. (1991) Sorption of divalent metals on calcite. *Geochim. Cosmochim. Acta*, **55**, 1549–62.

[*Manuscript received 10 March 1998: revised 3 August 1998*]